THE JOURNAL OF PHYSICAL CHEMISTRY B

Article

Cite This: J. Phys. Chem. B 2018, 122, 86−97

pubs.acs.org/JPCB

Experimental Evidence for Noncanonical Thymine Cation Radicals in the Gas Phase

Andy Dang,[†] Huong T. H. Nguyen,[†] Heather Ruiz,[‡] Elettra Piacentino,[‡] Victor Ryzhov,*[,‡] and František Tureček*[,†]

[†]Department of Chemistry, University of Washington, Bagley Hall, Box 351700, Seattle, Washington 98195-1700, United States

[‡]Department of Chemistry and Biochemistry, Northern Illinois University, DeKalb, Illinois 60115, United States

Supporting Information

ABSTRACT: Thymine cation radicals were generated in the gas phase by collision-induced intramolecular electron transfer in [Cu(2,2′:6,2″-terpyridine)(thymine)]$^{2+\bullet}$ complexes and characterized by ion−molecule reactions, UV−vis photodissociation action spectroscopy, and ab initio and density functional theory calculations. The experimental results indicated the formation of a tautomer mixture consisting chiefly (77%) of noncanonical tautomers with a C-7-H_2 group. The canonical 2,4-dioxo-N-1,N-3-H isomer was formed as a minor component at ca. 23%. Ab initio CCSD(T) calculations indicated that the canonical [thymine]$^{+\bullet}$ ion was not the lowest-energy isomer. This contrasts with neutral thymine, for which the canonical isomer is the lowest-energy structure. Exothermic unimolecular isomerization by a methyl hydrogen migration in the canonical [thymine]$^{+\bullet}$ ion required a low energy barrier, forming a C-7-H_2,O-4-H isomer. Noncanonical thymine tautomers with a C-7-H_2 group were also identified by calculations as low-energy isomers of 2′-deoxythymidine phosphate cation radicals. The relative energies of thymidine ion isomers were sensitive to the computational method used and were affected by solvation. The noncanonical [thymine]$^{+\bullet}$ ions have extremely low adiabatic recombination energies (RE_{adiab} < 5.9 eV), making them potential ionization hole traps in ionized nucleic acids.

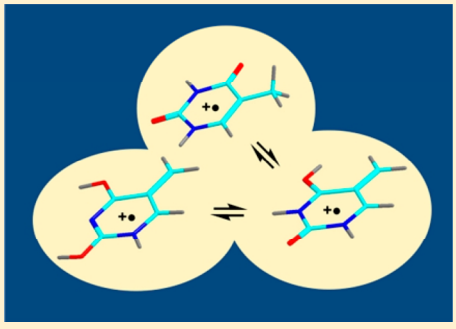

INTRODUCTION

DNA ionization triggers degradation chemical reactions that can lead to DNA damage such as nucleobase loss and strand breaks.[1] The processes involved in DNA ionization have been studied at several levels, ranging from individual nucleobases through nucleotides to double-stranded oligonucleotide DNA models.[2−4] A phenomenon of particular interest has been the propagation of the cation-radical defect (a "hole") from the initial site, generated randomly at a nucleobase, along the DNA strand. Model studies have tremendously contributed to our understanding of the hole migration at the nanoscale level. Nucleobase cation radicals have been generated by targeted photooxidation by intercalated transition metal complexes,[5] organic groups,[6] or photoinduced electron transfer.[7] Among the DNA nucleobases, thymine has the highest ionization energy (8.8−9.4 eV), as established by photoelectron spectroscopy,[8−10] photoionization,[11,12] and computational studies.[13−16] Perhaps even more relevant for solution studies, thymine also has the highest electrochemical oxidation potential among the DNA nucleobases.[17,18] These properties make the thymine cation radical a likely electron acceptor by transfer from other nucleobases, and because of its high ionization potential, thymine might be considered a nonreactive spacer in studies of hole propagation by hopping between guanine bases.[6] In contrast, recent studies of A-T-rich DNA models[19−24] demonstrated the high reactivity of the ionized thymine nucleobase. Reaction of thymidine with photoexcited 2-methyl-1,4-naphthoquinone[25,26] in the presence of molecular oxygen gave intermediates that were hydroperoxylated at the C-5 methyl group, indicating deprotonation followed by oxygen addition to the C-7-H_2 radical.[27] The methyl group is also a preferred site of attack by OH radicals, forming thymine C-7-H_2 radicals.[28] The reactivity of thymine cation radicals has been addressed by density functional theory (DFT) calculations in studies that focused on intra- and intermolecular proton transfer.[29−31] An important finding in these studies was the theoretical existence of a low-energy tautomer of [thymine]$^{+\bullet}$ that was separated from the canonical 2,4-dioxo form by a relatively low-energy barrier.[29]

Thymine cation radicals have been produced as transient species by photoionization[32,33] and radiolytic[34−36] or chemical oxidation[37−40] in solution, where they were exposed to solvents, additives, and side-reaction products. In contrast, the rarefied gas phase provides an ideal medium for studying isolated reactive species to investigate their intrinsic properties in the absence of solvent, counterions, and surfaces.[41] Among nucleobase radicals, hydrogen adducts of cytosine, adenine, and uracil have been generated in the gas phase by femtosecond electron transfer to the corresponding cations, and their structure, energetics, and unimolecular dissociations have been investigated.[42−44] Synthetic routes to gas-phase biomolecular cation radicals also

Received: October 5, 2017
Revised: November 19, 2017
Published: December 8, 2017

DOI: 10.1021/acs.jpcb.7b09872
J. Phys. Chem. B 2018, 122, 86−97

rely on reductive or oxidative electron transfer.[45,46] For example, intramolecular oxidation of the biomolecule (M) in a complex with a transition metal (Cu^{2+}, Fe^{3+}) and an auxiliary ligand such as 2:2′,6′:2″-terpyridine (terpy) has been used to produce gas-phase peptide and nucleobase cation radicals.[47,48] The oxidation is driven by collision-induced dissociation (CID) of a doubly charged complex generated by electrospray ionization and selected by mass, according to the equation

$$[Cu(terpy)(M)]^{2+\bullet} \rightarrow [Cu(terpy)]^{+} + M^{+\bullet} \quad (1)$$

Gas-phase chemistry analogous to eq 1 has been used to generate cation radicals of 9-methylguanine[49] and cytosine,[50] as well as the more complex systems of deoxyguanosine[51] and the Watson–Crick cytosine–guanine pair.[52] The mass-selected cation radicals generated by eq 1 chemistry have been characterized by specific radical and electron transfer ion–molecule reactions,[50] infrared multiphoton dissociation (IRMPD) action spectroscopy,[49−52] and single-photon UV–vis photodissociation action (UVPD) spectroscopy.[50] The action spectroscopy methods rely on resonant photon absorption by a gas-phase ion to induce dissociation ("action"), whereby the fragment ions formed are detected by mass spectrometry.[53] Action spectra can provide a detailed characterization of vibrational modes (IRMPD) or electronic excitations (UVPD) of the gas-phase ion that are used for structure assignment. In particular, action spectroscopy has been used to elucidate structures of isomeric cytosine cation radicals[50] and deoxyadenosine dinucleotides.[46] Here, we report the generation and structure elucidation of isomeric thymine cation radicals. The high ionization energy of thymine represents a potential challenge for the efficient generation of thymine cation radicals.[54] We show that thymine cation radicals produced in the gas phase exist in unexpected, low-energy tautomeric forms of potential relevance for the process of DNA ionization.

EXPERIMENTAL SECTION

Materials. Thymine, thymine-6,7,7,7-d_4, 2′-deoxythymidine, $Cu(NO_3)_2$, and 2,2′:6′,2″-terpyridine were purchased from Sigma-Aldrich (St. Louis, MO) and used as received. Stock solutions (1 mg mL^{-1}) of thymine and terpy were prepared in methanol, and those of thymidine and $Cu(NO_3)_2$ were made in water/methanol (50:50). The stock solutions of terpy and $Cu(NO_3)_2$ were combined in a 1:1 ratio and diluted 10-fold in methanol. An aliquot of this solution was combined with the thymine or thymidine solution, vortexed, and allowed to react for 10 min at room temperature. The resulting solution was diluted with methanol and used for direct infusion into the electrospray ion source.

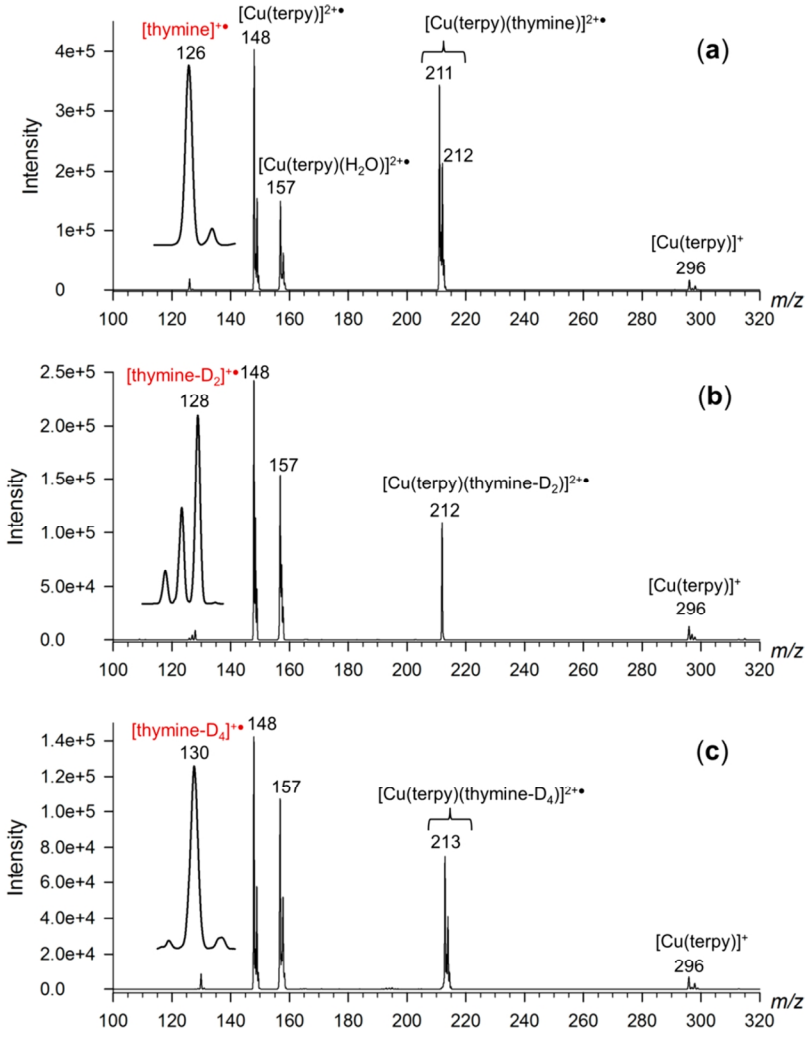

Figure 1. Collision-induced dissociation MS^2 spectra of (a) $[Cu(terpy)(thymine]^{2+\bullet}$ at m/z 211 and 212, (b) $[Cu(terpy)(thymine\text{-}1,3\text{-}d_2)]^{2+\bullet}$ at m/z 212 and 213, and (c) $[Cu(terpy)(thymine\text{-}6,7,7,7\text{-}d_4)]^{2+\bullet}$ at m/z 213 and 214.

DOI: 10.1021/acs.jpcb.7b09872
J. Phys. Chem. B 2018, 122, 86−97

Scheme 1. Formation of [Thymine]$^{+\bullet}$ Ions from Cu-terpy Complexes

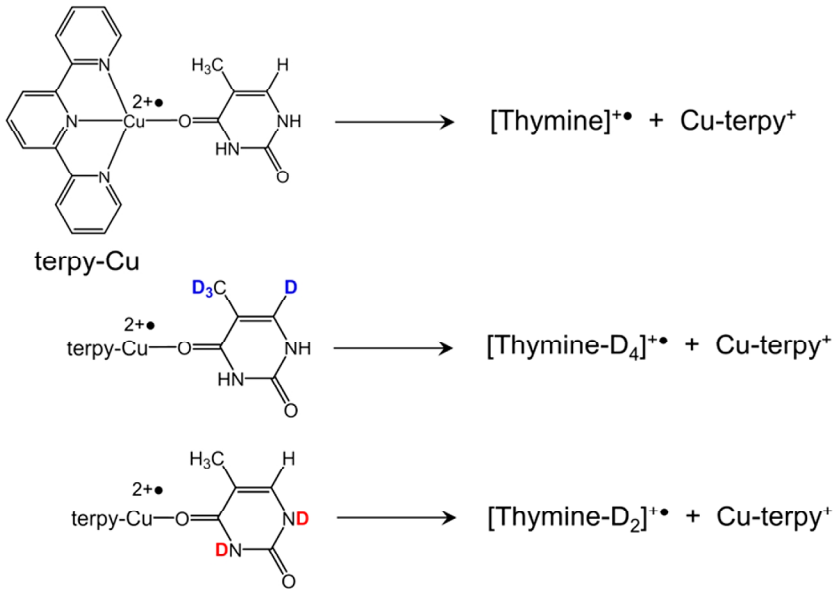

Methods. Mass spectra were measured on an LTQ-XL-ETD linear ion trap (Thermo Electron Fisher, San Jose, CA) furnished with a home-built microspray electrospray ion source. Photodissociation action spectra were measured as described previously.[55] Briefly, a laser beam from an EKSPLA NL301G Nd:YAG laser source (Altos Photonics, Bozeman, MT) was processed and mixed by an optical parametric oscillator (PG142C, Altos Photonics), and the output was focused into the linear ion trap to drive photodissociation of stored mass-selected [thymine]$^{+\bullet}$ ions. The laser optical parametric oscillator (OPO) operates at 20 Hz with a 3–6-ns pulse width. The laser power (0.52–12.69 mJ per pulse peak) was measured at each wavelength and used to normalize the photofragment ion intensities. The spectra were reproduced twice on different days. High-resolution mass spectra were measured on an Orbitrap Velos mass spectrometer (Thermo Electron Fisher) at a resolving power of 60000. Ion–molecule reactions of mass-selected [thymine]$^{+\bullet}$ ions were measured on a modified Bruker Esquire 3000 quadrupole ion trap mass spectrometer (Bruker Daltonics, Bremen, Germany) as described previously.[56] Furan, anisole, water, and acetic acid were introduced through a leak valve. The reaction time was defined by the delay between the ion isolation and product scans.

Calculations. Standard ab initio and density functional theory calculations were performed with the Gaussian 09 suite of programs.[57] The thymine ion and neutral geometries were optimized with the B3LYP,[58] M06-2X,[59] and ωB97X-D[60] hybrid DFT methods using the 6-311+G(2d,p) basis set. Local energy minima and first-order saddle points were characterized by harmonic frequency analysis as having the appropriate numbers of imaginary frequencies. Solvation energies were calculated with the M06-2X and ωB97X-D methods using the polarizable continuum model[61] available in Gaussian 09. Single-point energies were calculated using Møller–Plesset perturbation theory[62] truncated at second order [MP2(frozen core)] with the aug-cc-pVTZ basis set.[63] The MP2 energies were corrected for spin contamination by annihilation of higher spin states to provide spin-projected (PMP2) energies.[64,65] Alternatively, restricted open-shell calculations (ROMP2) were used for radicals.[66] Another set of single-point energies was obtained by coupled-cluster calculations with single, double, and disconnected triple excitations [CCSD(T)][67,68] using the aug-cc-pVDZ and 6-311++G(3df,2p) basis sets. The CCSD(T)/aug-cc-pVDZ calculations were expanded to aug-cc-PVTZ using the linear relationship E[CCSD(T)/aug-cc-pVTZ] ≈ E[CCSD(T)/aug-cc-pVDZ] + E[PMP2/aug-cc-pVTZ] − E[PMP2/aug-cc-pVDZ].

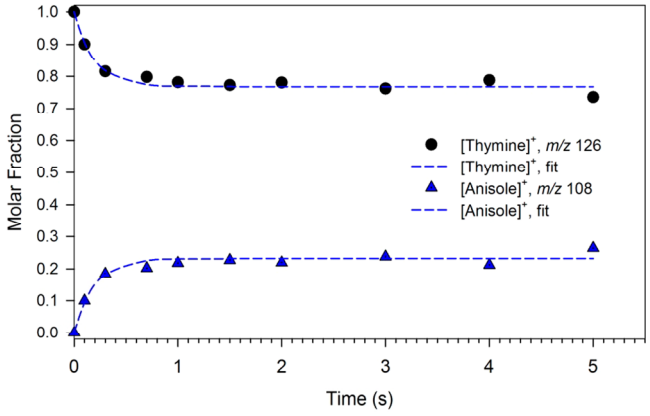

Figure 2. Kinetics of charge exchange between [thymine]$^{+\bullet}$ (m/z 126) and anisole, forming [anisole]$^{+\bullet}$ at m/z 108.

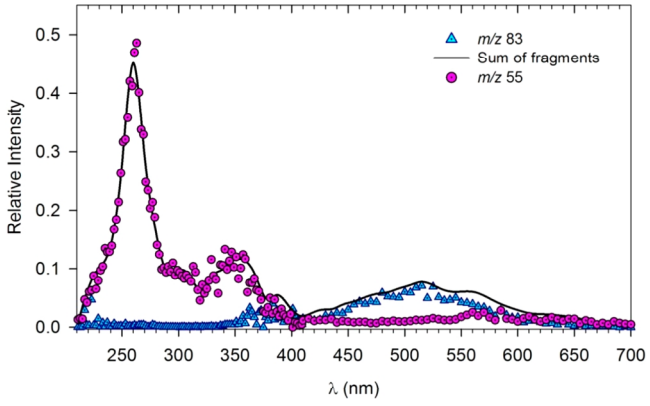

Figure 3. UV–vis photodissociation action spectrum of [thymine]$^{+\bullet}$ from [Cu(terpy)2′-thymine]$^{2+\bullet}$.

DOI: 10.1021/acs.jpcb.7b09872
J. Phys. Chem. B 2018, 122, 86–97

Excited states were treated by equation-of-motion- (EOM-) CCSD calculations[69,70] using the 6-31+G(d,p) basis set. Further sets of excitation energies and oscillator strength values were obtained by time-dependent DFT (TD-DFT) calculations[71] with the M06-2X and ωB97X-D methods using the 6-31+G(d,p) and 6-311+G(2d,p) basis sets. TD-DFT calculations of polyatomic radicals have been found to show only a very weak dependence on the basis set.[50,72,73] This was also the case for [thymine]$^{+\bullet}$, where excitation energies calculated by TD-DFT for 20 excited states with the 6-31+G(d,p) and 6-311+G(2d,p) basis sets showed a close correlation (r^2 = 0.9997) and small root-mean-square deviations [rmsd(ΔE_{exc}) = 0.046 eV, rmsd(λ) = 3.8 nm]. In contrast, EOM-CCSD-calculated excitation energies depend on the basis set, exhibiting a 0.1−0.2 eV downward shift upon use of a larger basis set compared [6-311++G(2d,p)] to 6-31+G(d,p).[72] Comparison of the TD-DFT and EOM-CCSD excitation wavelengths indicated a close correlation of the main lines (Figure S1, Supporting Information). The M06-2X excitations showed a red shift that was coincidentally of similar magnitude as that observed using EOM-CCSD calculations with a larger basis set. Therefore, TD-DFT M06-2X/6-31+G(d,p) calculations were used to calculate electronic transitions in multiple Boltzmann-weighed configurations of thermal (300 K) ions using the Newton-X program.[74] This generated vibronically corrected absorption spectra that are discussed later in this article. Rice−Ramsperger−Kassel−Marcus (RRKM) calculations of unimolecular rate constants[75] were performed using the QCEP program[76] that was recompiled for MS-DOS[77] and run under Windows 7. Rotational states were treated adiabatically, and the microcanonical rate constants $k(E,J)$, were Boltzmann averaged over the rotational state distribution at >298 K.

RESULTS AND DISCUSSION

Generation of Thymine Cation Radicals. Thymine cation radicals were produced by collision-induced dissociation (CID) of [Cu(terpy)thymine]$^{2+\bullet}$ ions that were formed by the electrospray of water/methanol solutions containing equimolar concentrations of $Cu(NO_3)_2$, terpy, and thymine (Figure 1a). The Cu complex was isolated as a mixture of ^{63}Cu and ^{65}Cu isotopologues, and its CID resulted in a major loss of neutral thymine, forming the [Cu(terpy)]$^{2+\bullet}$ ions (m/z 148 and 149 for the ^{63}Cu and ^{65}Cu isotopes, respectively; 64%) and the corresponding water adducts at m/z 157 and 158 (30%). The competitive collision-induced intramolecular electron transfer in [Cu(terpy)thymine]$^{2+\bullet}$ yielded the complementary [thymine]$^{+\bullet}$ (m/z 126) and [Cu(terpy)]$^{+}$ (m/z 296, 298) ions that were produced in a 6% relative fragment yield. The identity of the [thymine]$^{+\bullet}$ ion was supported by accurate mass measurements (measured 126.0427, theoretical 126.0424 for $C_5H_6N_2O_2^{+\bullet}$, error < 2.5 ppm). The branching ratio of the competing channels changed only very slightly (±0.2%) with the applied collision energy. CID with electron transfer provided a sufficient [thymine]$^{+\bullet}$ ion count for further multistep tandem mass spectrometry (MS^n) studies. H/D exchange in D_2O/CD_3OD solution and electrospray were used to generate [Cu(terpy)(thymine-d_2)]$^{2+\bullet}$ precursor ions, and upon mass isolation and CID, [thymine-d_2]$^{+\bullet}$ ions were obtained (Scheme 1, Figure 1b). [Thymine-d_4]$^{+\bullet}$ ions were prepared analogously in 5.7% yield from mass-selected [^{63}Cu(terpy)(thymine-d_4)]$^{2+\bullet}$ and [^{65}Cu(terpy)(thymine-d_4)]$^{2+\bullet}$ complexes using thymine-6,7,7,7-d_4 as the ligand (Figure 1c). The [thymine]$^{+\bullet}$ ions and their d_2 and d_4 analogues were characterized by multistep tandem mass spectrometry (CID-MS^3) spectra that showed loss of HNCO and (HNCO + CO) from [thymine]$^{+\bullet}$ and [thymine-6,7,7,7-d_4]$^{+\bullet}$ (Figure S2a−c, Supporting Information). These are also major dissociations upon electron ionization of gaseous thymine.[78−81] CID-MS^3 of [thymine-1,3-d_2]$^{+\bullet}$ resulted in loss of DNCO and HNCO in a 86:14 ratio (Figure S2b).

Ion−Molecule Reactions. The mass-selected and thermalized (300 K) [thymine]$^{+\bullet}$ ions were probed by ion−molecule

Table 1. Energies of Thymine Cation Radicals

isomer	relative energy[a] (kJ mol^{-1})				
	B3LYP/6-311+G(2d,p)	ωB97X-D	M06-2X	CCSD(T)/6-311++G(3df,2p)[b]	CCSD(T)/aug-cc-pVTZ[b,c]
1$^{+\bullet}$	0 (0)[d]	0 (0)[d]	0 (0)[d]	0 (0)[d]	0 (0)[d]
2$^{+\bullet}$	13	13	6	15	12
3$^{+\bullet}$	32	38	30	45	42
4$^{+\bullet}$	45	47	33	46	40
5$^{+\bullet}$	49	50	36	-	44
6$^{+\bullet}$	58	60	55	-	57
7$^{+\bullet}$	64	67	58	-	80
8$^{+\bullet}$	−26 (−21)[d]	−25 (−21)	−41 (−36)	−28 (−24)	−34 (−29)
9$^{+\bullet}$	−10 (−7)	−9 (−6)	−15 (−12)	−8 (−5)	−12 (−8)
10$^{+\bullet}$	1.5 (4.8)	1.9 (5.2)	−6 (−3)	−5 (−1.6)	−7 (−4.1)
11$^{+\bullet}$	10 (15)	13 (17)	−3 (1.3)	8 (12)	2 (6)
12$^{+\bullet}$	158	181	179	157	155
13$^{+\bullet}$	174	192	189	189	185
TS1	104	110	111	113	107
TS2	143	146	137	144	136
TS3	140	144	134	139	131
TS4	170	207	207	191	187
TS5	172	190	189	l80	175
TS6	264	263	250	-	-
$C_4H_5NO^{+\bullet}$ + O=C=NH	187	208	216	198	200
$C_3H_5N^{+\bullet}$ + CO + O=C=NH	182	228	212	192	193
$C_3H_5N^{+\bullet}$ + O=C=N−CH=O	182	222	217	207	208

[a]Including B3LYP/6-311+G(2d,p) zero-point energy corrections and referring to 0 K unless stated otherwise. [b]Single-point energies on MP2(full)/6-31G(d,p)-optimized geometries. [c]From basis set expansion of aug-cc-pVDZ → aug-cc-pVTZ. [d]Values in parentheses are relative free energies at 310 K.

DOI: 10.1021/acs.jpcb.7b09872
J. Phys. Chem. B 2018, 122, 86−97

reactions. Exothermic charge-transfer ion–molecule reactions typically proceed at the collision rate[82] and provide a sensitive probe of ion structure in situations where isomeric ions differ in their adiabatic recombination energies (REs).[50] Previous photoelectron spectroscopic measurements[8−10] established the adiabatic ionization energy of gas-phase thymine as 8.8–9.40 eV, which is equal to the absolute value of the RE. The gas-phase charge-exchange reaction of $[thymine]^{+\bullet}$ with gaseous furan (IE = 8.88 eV) did not proceed at a measurable rate, as evidenced by the fact that <1% of $C_4H_4O^{+\bullet}$ ions formed. Upon long reaction times (5 s), we observed a minor (2%) $C_4H_5O^+$ product from proton transfer to furan. Interestingly, the charge-exchange reaction of $[thymine]^{+\bullet}$ with gaseous anisole (IE = 8.42 eV) proceeded incompletely (Figure 2). The relative intensities of the $[thymine]^{+\bullet}$ (m/z 126) and $[anisole]^{+\bullet}$ (m/z 108) ions showed a bimodal time course that was fitted with an exponential equation for the $[thymine]^{+\bullet}$ relative intensity $I(t)$: $I(t) = I_0(0.77 + 0.23e^{-5.15t})$, giving a 1.6% root-mean-square deviation (rmsd). This left 77% nonreactive $[thymine]^{+\bullet}$ ions after ca. 1 s. This surprising result indicated that the population of $[thymine]^{+\bullet}$ produced from the $[Cu(terpy)thymine]^{2+\bullet}$ complex consisted of only a minor fraction of isomers with RE > 8.42 eV, whereas the major fraction of isomers had low recombination energies preventing charge transfer to anisole.

To investigate these new isomers, we performed additional ion–molecule reactions investigating proton transfer of $[thymine\text{-}1,3\text{-}d_2]^{+\bullet}$ and $[thymine\text{-}6,7,7,7\text{-}d_4]^{+\bullet}$ with gaseous water and acetic acid. $[Thymine\text{-}1,3\text{-}d_2]^{+\bullet}$, with a canonical 2,4-dioxo structure, has the N-1-D and N-3-D in exchangeable positions and was expected to undergo gas-phase D/H exchange, gradually forming $[thymine\text{-}d_1]^{+\bullet}$ and $[thymine]^{+\bullet}$ ions. Figure S3 shows the time course of the D/H exchange reaction with residual water that was measured in the linear ion trap and can be expressed by the following pseudo-first-order kinetic equation: $I(thymine\text{-}d_2) = I_0e^{-0.135t}$ with rmsd = 2.3%. These experiments established that the water partial pressure in the ion trap was sufficient to promote D/H exchange in exchangeable positions of the trapped ions.

In contrast, the canonical 2,4-dioxo isomer of $[thymine\text{-}6,7,7,7\text{-}d_4]^{+\bullet}$ has the deuterium in nonexchangeable C–D positions and was not expected to undergo D/H exchange with water vapor. Nevertheless, the $[thymine\text{-}6,7,7,7\text{-}d_4]^{+\bullet}$ ion was found to undergo slow D/H exchange in the gas-phase reaction with water and acetic acid, forming the d_3 isotopologue (Figure S4). This result indicates that a fraction of the $[thymine\text{-}6,7,7,7\text{-}d_4]^{+\bullet}$ ions formed from the $[Cu(terpy)]^{2+\bullet}$ complex did not have the canonical structure but rather underwent a prototropic rearrangement that moved the CD_3 or 6-D atoms into an exchangeable position (O-2 or O-4). In addition, these isomers must have recombination energies of <8.4 eV to be consistent with the above-mentioned charge-exchange measurements. Considering the 0.23 mole fraction of canonical $[6,7,7,7\text{-}d_4]$-2,4-dioxo isomer that cannot undergo D/H exchange, the $[thymine\text{-}6,7,7,7\text{-}d_4]^{+\bullet}$ mole fraction from D/H exchange with water was fitted with the bimodal curve $I(t) = I_0(0.77e^{-0.033t} + 0.23)$ with rmsd = 0.9%. Independent D/H exchange measurements with water and acetic acid vapor in a three-dimensional ion trap yielded very similar fits (Figure S4).

UV–Vis Action Spectroscopy. To further characterize the $[thymine]^{+\bullet}$ ions, we obtained photodissociation action spectra that were collected in the 210–700-nm range (Figure 3). Photodissociation proceeded in two major channels, which were the loss of HNCO and the loss of (HNCO + CO), forming the m/z 83 and m/z 55 fragment ions, respectively. Note that these fragments were also observed upon CID of $[thymine]^{+\bullet}$ (Figure S2a). The wavelength profiles of the relative intensities of the m/z 83 and m/z 55 fragment ions overlapped but showed different maxima. The m/z 83 ion exhibited a broad band with a maximum at 520 nm. The m/z 55 ion exhibited multiple bands: a weak broad band with a maximum at 580, bands at 460 and 350 nm, and a strong UV band at 260 nm. The bands in the visible and near-UV regions are absent in the UV spectrum of neutral and protonated thymine[83] and represent a signature of the cation-radical chromophores. To interpret the action spectrum of $[thymine]^{+\bullet}$, we performed extensive ab initio calculations of isomeric ion structures and excitation energies, as described in the next sections.

Thymine Cation Radical Structures. Thymine cation radicals can form several tautomers including those in which a hydrogen from the CH_3 group has migrated into a ring position.[29] We obtained optimized structures and DFT relative energies of 18 $[thymine]^{+\bullet}$ isomers (Table 1), and 11 low-energy structures were evaluated by CCSD(T) single-point energy calculations. Structures of the low-energy isomers are shown in Figure 4; those of the others ($\mathbf{14}^{+\bullet}$–$\mathbf{20}^{+\bullet}$) are shown in Figure S5 of the Supporting Information. The canonical 2,4-dioxo tautomer $\mathbf{1}^{+\bullet}$ was the lowest-energy structure among the cation radicals having the CH_3 group ($\mathbf{1}^{+\bullet}$–$\mathbf{7}^{+\bullet}$). This is analogous to

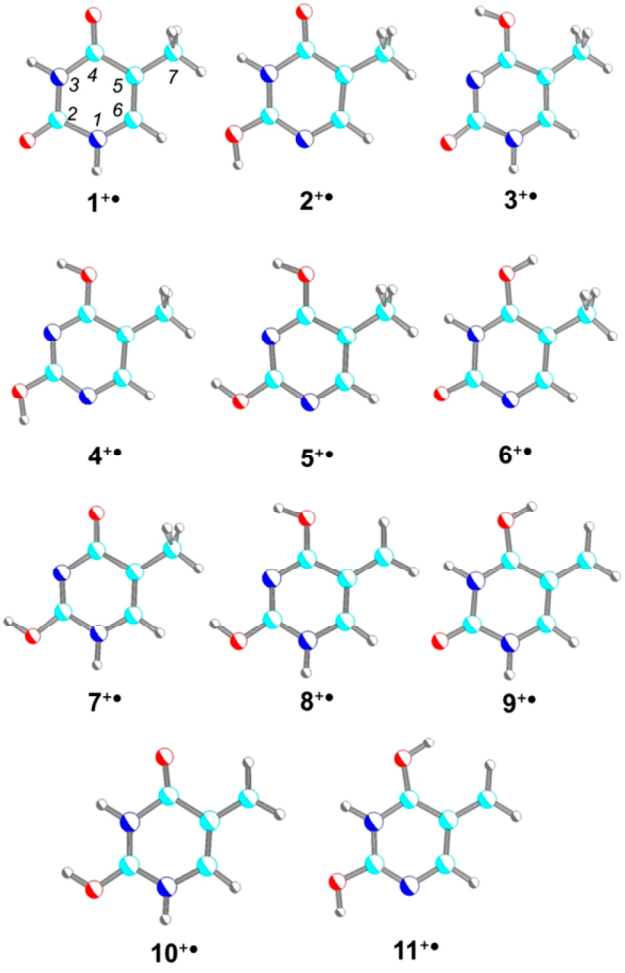

Figure 4. M06-2X/6-31+G(d,p)-optimized structures of $[thymine]^{+\bullet}$ cation radicals. Atom color coding: turquoise, C; gray, H; blue, N; red, O.

DOI: 10.1021/acs.jpcb.7b09872
J. Phys. Chem. B 2018, 122, 86–97

Table 2. Relative and Adiabatic Ionization Energies of Neutral Thymine Isomers

	relative energy[a] (kJ mol^{-1})				
species	B3LYP[b]	M06-2X[b]	ωB97X-D[b]	CCSD(T)[c]	CCSD(T)[d]
1	0 (842)[e]	0 (857)	0 (844)	0 (854)	0 (860)
2	45 (810)	38 (826)	47 (810)	42 (827)	39 (833)
4	55 (832)	40 (850)	57 (833)	50 (851)	44 (856)
8	267 (550)	265 (551)	286 (533)	276 (550)	269 (557)
10	280 (564)	287 (564)	302 (544)	287 (563)	282 (571)
11	288 (565)	287 (568)	308 (549)	299 (563)	291 (570)

[a]Including B3LYP zero-point vibrational energies and referring to 0 K. [b]Calculations with the 6-311+G(2dp) basis set. [c]From single-point calculations with the 6-311++G(3df,2p) basis set. [d]From effective CCSD(T)/aug-cc-pVTZ single-point calculations. [e]Adiabatic ionization energies in kJ mol^{-1} in parentheses.

neutral thymine, for which the canonical form is the most stable isomer in the gas phase.[84,85] In contrast, four isomers having the C-7-H_2 group, **8**$^{+\bullet}$–**11**$^{+\bullet}$, had a free energy that was lower than or comparable to that of **1**$^{+\bullet}$. The lowest-energy isomer, **8**$^{+\bullet}$, having the N-1-H, O-2-H, and O-4-H protonation pattern, was 24 kJ mol^{-1} more stable than **1**$^{+\bullet}$, according to the calculated ΔG°_{g} at the experimental temperature of 310 K. Two other isomers that had free energies comparable to that of **1**$^{+\bullet}$ were **9**$^{+\bullet}$, with the N-1-H, N-3-H, and O-4-H protonation pattern, and **10**$^{+\bullet}$, with the N-1-H, O-2-H, and N-3-H protonation pattern. Another isomer (**11**$^{+\bullet}$) was 12 kJ mol^{-1} less stable than **1**$^{+\bullet}$ at 310 K.

In contrast to the cation radicals, neutral thymine tautomers **8**, **10**, and **11**, with the C-7-H_2 group, were >260 kJ mol^{-1} less stable than **1** (Table 2). Neutral isomer **9** was found to be a transition state (TS) that collapsed to **1** upon O–H rotation. The high energies of neutral species **8**, **10**, and **11** combined with the low energies of the respective cation radicals resulted in extremely low (<5.9 eV) adiabatic recombination energies for the cation radicals (Table 2). This result is consistent with the charge-exchange experiments, in which 77% of [thymine]$^{+\bullet}$ cation radicals were found to have very low ionization energies. Considering that the calculated adiabatic recombination energies of **8**$^{+\bullet}$, **9**$^{+\bullet}$, and **11**$^{+\bullet}$ are well below those of volatile organic and inorganic atoms and molecules with the exception of alkali metals, experimental determination of the RE_{adiab} values by charge-exchange bracketing of [thymine]$^{+\bullet}$ ions would be difficult.

Electronic Excitations. We used the optimized structures of the low-energy isomers **1**$^{+\bullet}$ and **8**$^{+\bullet}$–**11**$^{+\bullet}$ to calculate the excitation energies and oscillator strengths and obtain absorption spectra for comparison with the experimental photodissociation action spectrum of [thymine]$^{+\bullet}$. The spectra of all of the low-energy isomers showed a major band at 245–270 nm, although this band was notably weaker in the spectrum of **1**$^{+\bullet}$ (Figure 5a). This band appears at 260 nm in the action spectrum of [thymine]$^{+\bullet}$ and cannot be used to represent a specific isomer. The spectra of **8**$^{+\bullet}$ and **10**$^{+\bullet}$ are the only ones showing a distinct band at 330–360 nm to match the 330–360-nm band in the action spectrum of [thymine]$^{+\bullet}$ (Figure 5b,d). This indicates that **8**$^{+\bullet}$ or **10**$^{+\bullet}$ or both are present in the [thymine]$^{+\bullet}$ ion population. The long-wavelength bands in the visible region of the spectrum are also diagnostic. The broad band at 550–600 nm represented by the m/z 55 photodissociation channel in the action spectrum can be matched by the 550- and 615-nm bands in the absorption spectra of **1**$^{+\bullet}$ and **9**$^{+\bullet}$ (panels a and c, respectively, of Figure 5). Likewise, the 500-nm band represented by the m/z 83 photodissociation channel in the action spectrum finds analogous bands in the spectra of **8**$^{+\bullet}$ and **11**$^{+\bullet}$ (panels b and e, respectively, of Figure 5). The minor band

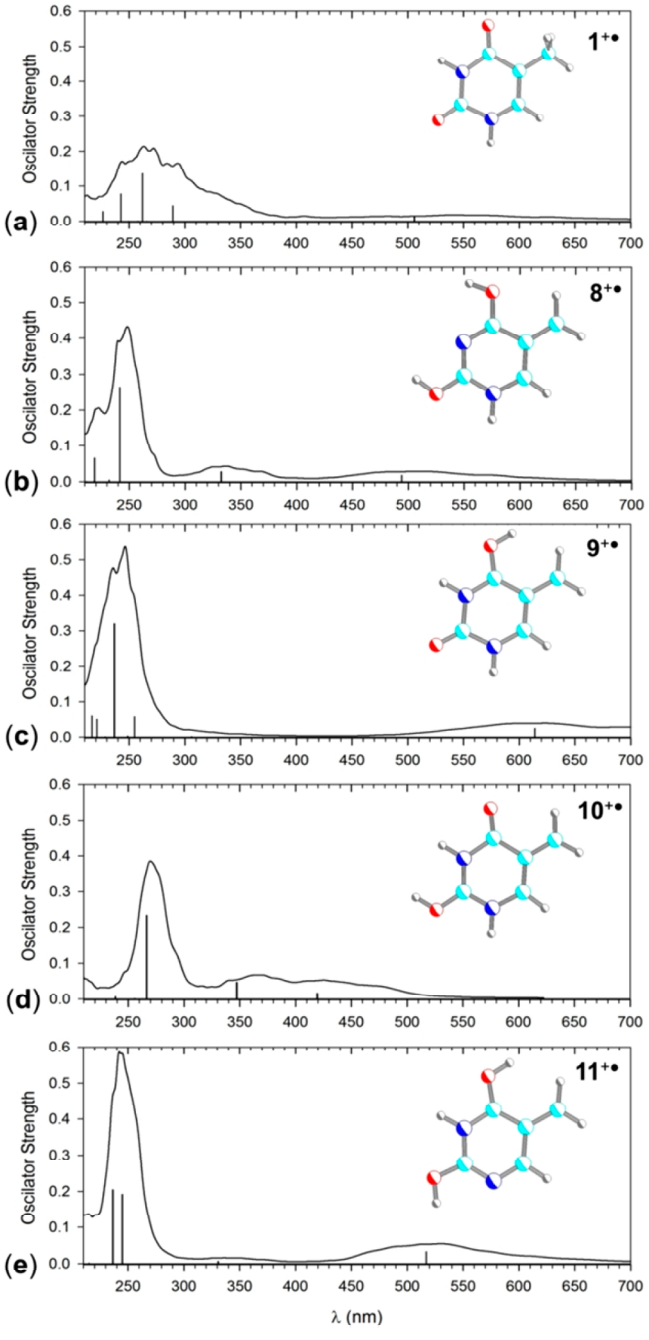

Figure 5. Vibronically broadened (300 K) TD-DFT M06-2X/6-31+G(d,p) absorption spectra of (a) **1**$^{+\bullet}$, (b) **8**$^{+\bullet}$, (c) **9**$^{+\bullet}$, (d) **10**$^{+\bullet}$, and (e) **11**$^{+\bullet}$. The bars represent the calculated vertical transitions.

DOI: 10.1021/acs.jpcb.7b09872
J. Phys. Chem. B 2018, 122, 86–97

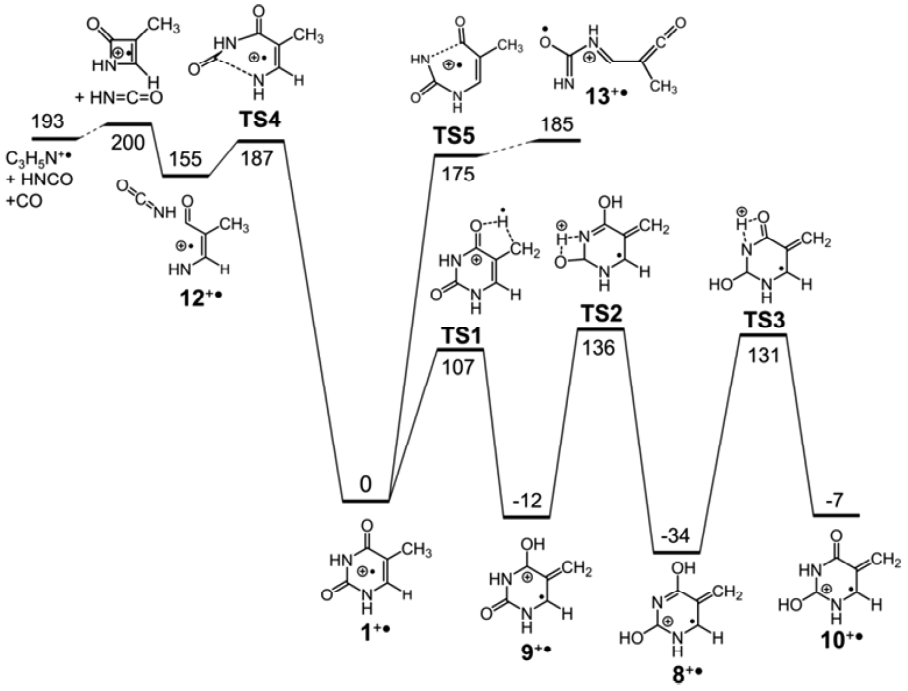

Figure 6. Potential energy surface (kJ mol^{-1}) for isomerizations and dissociations of $\mathbf{1}^{+\bullet}$. Energies relative to $\mathbf{1}^{+\bullet}$ are from effective CCSD(T)/aug-cc-pVTZ calculations. For energies from the other calculations, see Table 1.

at 460 nm represented by the m/z 55 photodissociation channel in the action spectrum has an analogue in the absorption spectrum of $\mathbf{10}^{+\bullet}$ (Figure 5d). From this comparison, it is clear that the action spectrum of [thymine]$^{+\bullet}$ cannot be represented by a spectrum of a single ion isomer, indicating that the gas-phase ions were a mixture of isomers. This conclusion is consistent with the results of the ion−molecule reactions, as described above. We did not attempt to quantify the fractions of the individual noncanonical [thymine] $^{+\bullet}$ isomers whose spectra compose the action spectrum. This is because photodissociation, especially at short wavelengths (210−250 nm, ≥5 eV photon energy), could lead to consecutive dissociations of the primary photofragments to yield low-mass secondary ions that would fall below the low-mass cutoff of the ion trap and thus be undetectable in the mass spectra. This could skew the band intensities and affect quantitation.

Potential Energy Surface for [Thymine]$^{+\bullet}$. The experimental evidence for the formation of [thymine]$^{+\bullet}$ isomers other than the canonical form $\mathbf{1}^{+\bullet}$ raised the question of the stage at which the isomerization occurs. Neutral thymine is present in solution in its canonical 2,4-dixo form. Isomerization could potentially occur in solution upon binding in the [Cu(terpy)-(thymine)]$^{2+\bullet}$ complex or upon collisional activation in the gas phase. We address the latter possibility first. The potential energy surface for the important steps in the isomerization and dissociation of gas-phase $\mathbf{1}^{+\bullet}$ was obtained by CCSD(T) single-point energy calculations including zero-point vibrational energy corrections (Figure 6). For energies calculated at other levels of theory, see Table 1. For optimized structures of transition states, see Figure S6 (Supporting Information). Whereas isomerizations of $\mathbf{1}^{+\bullet}$ to $\mathbf{8}^{+\bullet}$−$\mathbf{10}^{+\bullet}$ were found to be exothermic, the initial step, which is H-atom migration from the methyl group to O-4 forming $\mathbf{9}^{+\bullet}$, required that an energy barrier be overcome in **TS1**. The energy barriers for consecutive H-atom migrations, interconnecting $\mathbf{9}^{+\bullet}$ with $\mathbf{8}^{+\bullet}$ and $\mathbf{8}^{+\bullet}$ with $\mathbf{10}^{+\bullet}$ (**TS2** and **TS3**,

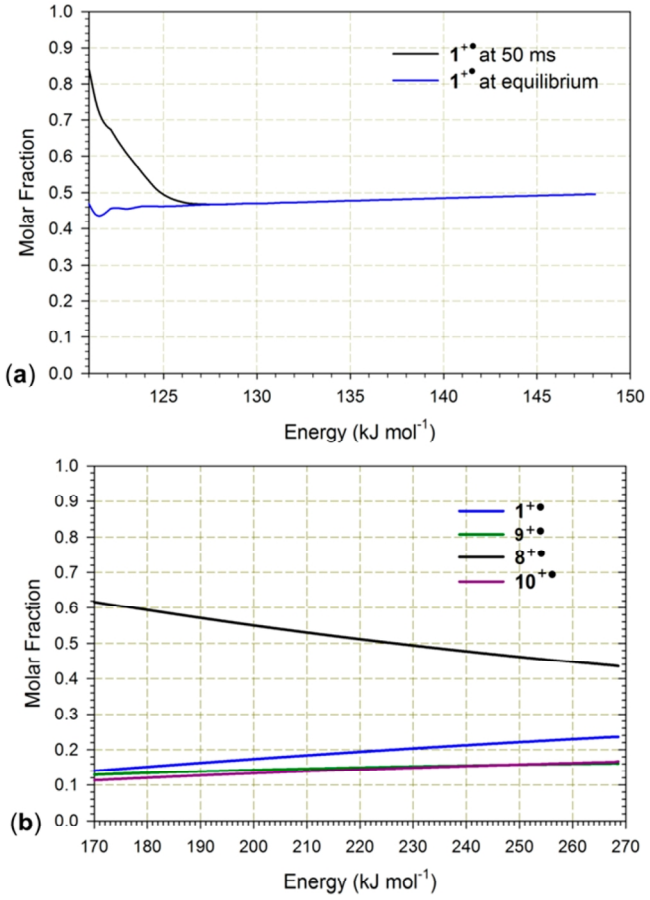

Figure 7. Mole fractions of $\mathbf{1}^{+\bullet}$, $\mathbf{8}^{+\bullet}$, $\mathbf{9}^{+\bullet}$, and $\mathbf{10}^{+\bullet}$ from RRKM calculations of isomerization rate constants. (a) Kinetics of reversible $\mathbf{1}^{+\bullet} \leftrightarrow \mathbf{9}^{+\bullet}$ isomerization at low internal energies and (b) equilibrium mole fractions at high internal energies.

DOI: 10.1021/acs.jpcb.7b09872
J. Phys. Chem. B 2018, 122, 86−97

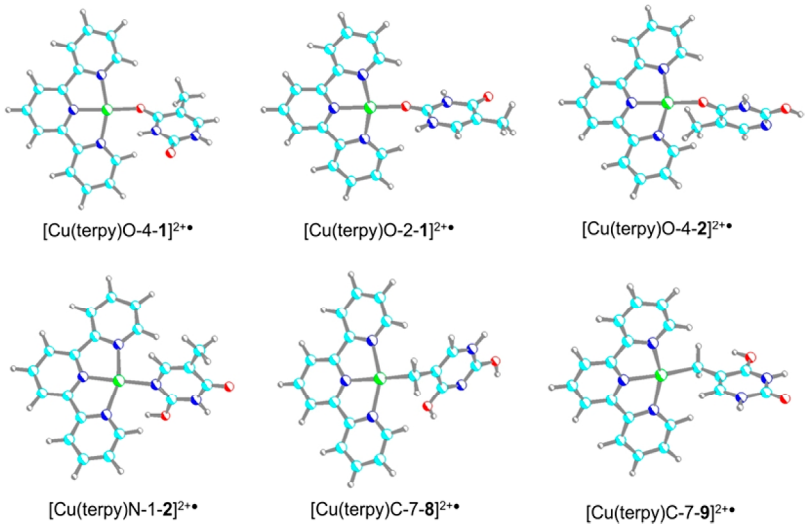

Figure 8. M06-2X/6-311+G(2d,p)-optimized structures of $[Cu(terpy)(thymine)]^{2+\bullet}$ complexes.

respectively), were found to be 26−30 kJ mol^{-1} higher than that for **TS1**.

In contrast, energy barriers to a ring opening en route to dissociation had substantially higher TS energies for cleavage of the N-1−C-2 and N-3−C-4 bonds. The transition state for the N-1−C-2 bond cleavage (**TS4**) was 188 kJ mol^{-1} relative to that of $\mathbf{1}^{+\bullet}$, leading to a complex of O═C═NH and $C_4H_5NO^{+\bullet}$ ($\mathbf{12}^{+\bullet}$) at 156 kJ mol^{-1} (Figure 6, Table 1). The transition state for the N-3−C-4 bond cleavage (**TS5**) was 175 kJ mol^{-1} relative to thhat of $\mathbf{1}^{+\bullet}$, possibly forming a high-energy intermediate ($\mathbf{13}^{+\bullet}$) after rotation about the N-1−C-6 bond. The thresholds for the formation of the observed dissociation products ($C_4H_5NO^{+\bullet}$ + O═C═NH), ($C_3H_4N^{+\bullet}$ + CO + O═C═NH), and ($C_3H_4N^{+\bullet}$ + O═CH−N═C═O), were 200, 193, and 208 kJ mol^{-1}, respectively, relative to the thresholds for $\mathbf{1}^{+\bullet}$. Ring opening by N-1−C-2 bond cleavage in $\mathbf{9}^{+\bullet}$ was unfavorable, requiring 260 kJ mol^{-1} in the pertinent transition state (**TS6**, Table 1).

The kinetics for a reversible isomerization of $\mathbf{1}^{+\bullet}$ to $\mathbf{9}^{+\bullet}$ and further to $\mathbf{8}^{+\bullet}$ and $\mathbf{10}^{+\bullet}$ was evaluated from unimolecular rate constants obtained by RRKM calculations (Figure S7, Supporting Information). At internal energies between E(**TS1**) and E(**TS2**), $\mathbf{1}^{+\bullet}$ rapidly isomerized to $\mathbf{9}^{+\bullet}$, reaching an equilibrium within 50 ms at internal energies greater than 128 kJ mol^{-1} (Figure 7a). Note that 50 ms is a benchmark ion residence time in the ion trap. Interestingly, although $\mathbf{9}^{+\bullet}$ had a lower ΔH_0 value than $\mathbf{1}^{+\bullet}$, the equilibrium fraction of $\mathbf{9}^{+\bullet}$ was close to 50% and further decreased with increasing internal energy. This is caused by a higher density of vibrational states in $\mathbf{1}^{+\bullet}$, increasing its entropy. The $\mathbf{1}^{+\bullet} \rightarrow \mathbf{9}^{+\bullet}$ isomerization showed a substantial combined isotope effect that slowed the isomerization of 6,7,7,7-d_4-$\mathbf{1}^{+\bullet}$ more than 5-fold at internal energies below 150 kJ mol^{-1} (Figure S8, Supporting Information). At internal energies above 170 kJ mol^{-1}, the subsequent isomerizations of $\mathbf{9}^{+\bullet}$, $\mathbf{8}^{+\bullet}$, and $\mathbf{10}^{+\bullet}$ also became fast, allowing the system to reach an equilibrium including $\mathbf{1}^{+\bullet}$, $\mathbf{8}^{+\bullet}$, $\mathbf{9}^{+\bullet}$, and $\mathbf{10}^{+\bullet}$. The equilibrium mole fractions were found to be energy-dependent (Figure 7b), whereby that of $\mathbf{1}^{+\bullet}$ was increasing whereas that of $\mathbf{8}^{+\bullet}$ was decreasing at high internal energies. The N-1−C-2 and N-3−C-4 modes of ring opening became kinetically relevant at internal energies of >190 kJ mol^{-1}, where the rate constants reached 14 s^{-1} for 50% reaction at 50 ms (Figure S7). The high threshold energy for the ring opening explains why $\mathbf{1}^{+\bullet}$ can undergo extensive isomerization by reversible hydrogen migrations to generate a mixture of nondissociating $[thymine]^{+\bullet}$ ions. The RRKM kinetics also suggest that the dissociation of thermal $[thymine]^{+\bullet}$ having a mean internal energy of 24 kJ mol^{-1} at 310 K can be promoted by an absorption of >176 kJ mol^{-1} energy, corresponding to a single 680-nm photon.

Formation of $[Thymine]^{+\bullet}$ from the $[Cu(terpy)(thymine)]^{2+\bullet}$ Complex. The formation of unusual $[thymine]^{+\bullet}$ isomers upon CID of the $[Cu(terpy)(thymine)]^{2+\bullet}$ complex also raised the question of whether thymine coordination to Cu^{2+} in solution could lead to isomerization. We investigated by DFT calculations the relative energies of several $[Cu(terpy)(thymine)]^{2+\bullet}$ complexes in which the thymine ligands were different tautomers of the neutral molecule (Figure 8, Table 3). According to these calculations, the complex with an O-4-linked **1**, $[Cu(terpy)(O\text{-}4\text{-}\mathbf{1})]^{2+\bullet}$, was the lowest-energy structure in both the gas phase and aqueous and methanol solutions, followed by the complexes with an O-2-linked **1** and an O-4-linked **2**. In contrast, Cu(terpy) complexes with **8**, **9**, and **10** were >120 kJ mol^{-1} less stable than $[Cu(terpy)(O\text{-}4\text{-}\mathbf{1})]^{2+\bullet}$ and were unlikely to be present under equilibrium conditions in solution or formed by electrospray in the gas phase. We conclude that the formation of gas-phase $\mathbf{8}^{+\bullet}$−$\mathbf{11}^{+\bullet}$ most likely occurs as a result of collisional excitation and dissociation of the

Table 3. Relative Energies of $[Cu(terpy)(thymine)]^{2+\bullet}$ Complexes

	relative energy[a] (kJ mol^{-1})		
complex	B3LYP[b]	M06-2X[b]	ωB97X-D[b]
$[Cu(terpy)\rightarrow O\text{-}4\text{-}\mathbf{1}]^{2+\bullet}$	0	0 (0)[c]	0 (0)
$[Cu(terpy)\rightarrow O\text{-}2\text{-}\mathbf{1}]^{2+\bullet}$	17	16 (7)	20 (12)
$[Cu(terpy)\rightarrow O\text{-}4\text{-}\mathbf{2}]^{2+\bullet}$	36	7 (31)	19 (43)
$[Cu(terpy)\rightarrow N\text{-}1\text{-}\mathbf{2}]^{2+\bullet}$	86	76 (49)	78 (49)
$[Cu(terpy)\rightarrow N\text{-}3\text{-}\mathbf{9}]^{2+\bullet}$	120	145 (182)	125 (159)
$[Cu(terpy)\rightarrow C\text{-}7\text{-}\mathbf{9}]^{2+\bullet}$	130	128 (159)	125 (155)
$[Cu(terpy)\rightarrow C\text{-}7\text{-}\mathbf{8}]^{2+\bullet}$	154	159 (158)	145 (142)

[a]Including B3LYP/6-311+G(2d,p) zero-point energy corrections and referring to 0 K. [b]Calculations with the 6-311+G(2d,p) basis set. [c]Values in parentheses include solvation energies in the polarizable continuum of water.

DOI: 10.1021/acs.jpcb.7b09872
J. Phys. Chem. B 2018, 122, 86−97

[Cu(terpy)(thymine]$^{2+\bullet}$ complex that produces a fraction of [thymine]$^{+\bullet}$ ions with internal energies of >128 kJ mol^{-1} for kinetically relevant isomerization.

Thymidine Cation Radicals. We attempted to generate 2′-deoxythymidine cation radicals by collision-induced intramolecular electron transfer in the [Cu(terpy)(thymidine)]$^{2+\bullet}$ complex. The precursor ion was successfully made by electrospray ionization (m/z 269 and 271 for the ^{63}Cu and ^{65}Cu isotopes, respectively). However, CID of [Cu(terpy)(thymidine)]$^{2+\bullet}$ resulted in a dissociation of the *N*-glycosidic bond forming the complementary deoxyribosyl ($C_5H_9O_3^+$, m/z 117) and [Cu(terpy)(thymine)]$^{+\bullet}$ (m/z 421) singly charged fragment ions (Figure S9a, Supporting Information). The major CID product was the [Cu(terpy)(thymine)]$^{2+\bullet}$ ion (m/z 211), which, upon mass isolation and CID-MS^3 gave the [thymine]$^{+\bullet}$ ion, which, according to its UVPD and CID spectra was identical to the ion formed directly from the doubly charged thymine complex (Figure S9b, Supporting Information). The unequivocal course of dissociation of the [Cu(terpy)(thymidine)]$^{2+\bullet}$ complex indicates that the cleavage of the 2′-deoxythymidine glycosidic bond is energetically more favorable than the electron-transfer reaction forming [thymidine]$^{+\bullet}$ and [Cu(terpy)]$^+$ ions.

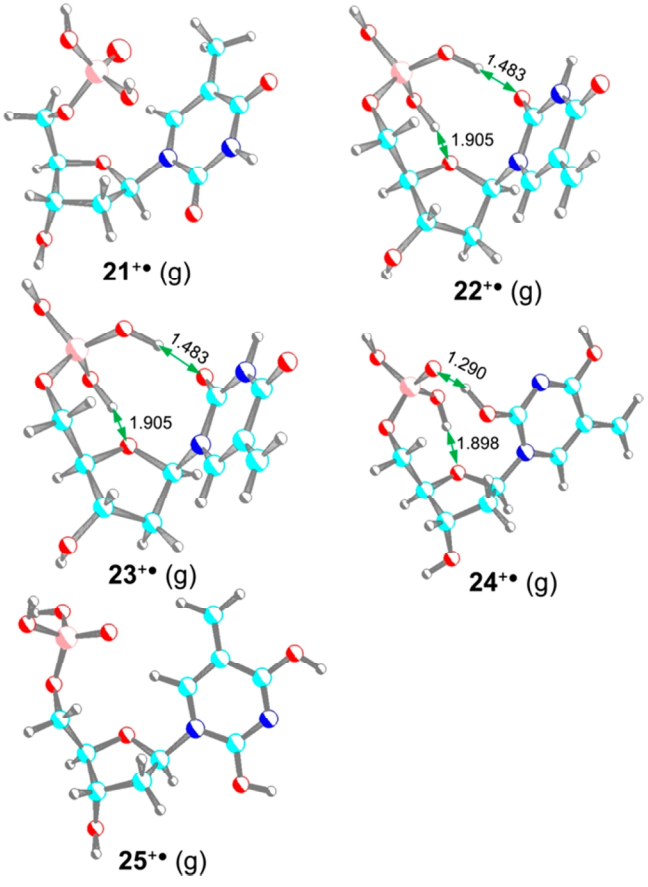

Figure 9. M06-2X/6-311+G(2d,p)-optimized structures of [2′-deoxythymidine phosphate]$^{+\bullet}$ isomers.

Thymidine Isomerization in Ionized Nucleotides. The existence of low-energy [thymine]$^{+\bullet}$ isomers could have a serious effect on charge transfer in ionized oligonucleotides. Because the recombination energies of **8**$^{+\bullet}$**–11**$^{+\bullet}$ are extremely low, in fact, much lower than the RE_{adiab} values of the other nucleobases, thymine ionization and isomerization would trap the hole at the thymine residue, providing a C-7-H_2 radical group for thymine-specific reactions.[19−24] To address this point, we investigated by DFT and ab initio computations the structures and relative energies of 2′-deoxythymidine phosphate cation radicals, both in the gas phase and in the polarizable dielectric of the surrounding water continuum. The ion relative energies, represented by the lowest-energy conformers **21**$^{+\bullet}$**–25**$^{+\bullet}$ (Figure 9), were found to depend on the computational method and also to be affected by entropies and solvent effects (Table 4). The canonical tautomer **21**$^{+\bullet}$ marginally had the lowest free energy ($\Delta G^\circ_{g,298}$) among the 2′-deoxythymidine phosphate isomers in the gas phase, chiefly because of its high vibrational entropy at 298 K. However, the $\Delta G^\circ_{g,298}$ values for **21**$^{+\bullet}$ and the C-7-H_2 tautomers **23**$^{+\bullet}$ and **24**$^{+\bullet}$ were as close as 2 kJ mol^{-1} (Table 4). Solvation by water favored the C-7-H_2 tautomer **22**$^{+\bullet}$, whose $\Delta G^\circ_{g,298}$ value was very close to those of **21**$^{+\bullet}$ and **24**$^{+\bullet}$. The calculations indicated that the relative stabilities of thymidine tautomers are extremely sensitive to the local environment and solvent. To resolve this issue, a dedicated computational study of cation-radical A−T pairs in oligonucleotides is needed; however, this exceeds the scope of this work. A conspicuous feature of thymidine cation-radical structures displaying strong intramolecular hydrogen bonds is the spontaneous migration of a thymine hydroxyl proton to the phosphate group, forming distonic ions **22**$^{+\bullet}$**–24**$^{+\bullet}$. These ions are expected to behave as thymine radicals and to undergo typical reactions triggered by oxygen addition to the C-7-H_2 group. The internal prototropic isomerization in **22**$^{+\bullet}$**–24**$^{+\bullet}$ is an alternative to external proton transfer from ionized thymine to the surrounding water molecules, as suggested previously.[24]

CONCLUSIONS

The experimental and computational results presented in this article point to the existence of noncanonical [thymine]$^{+\bullet}$ isomers having the C-7-H_2 group. The new isomers are formed as major products by intramolecular electron transfer in gas-phase metal−thymine complexes and represent the lowest-energy structures that are more stable than the canonical 2,4-dioxo-N-1,N-3-H form. Theoretical calculations also predict the

Table 4. Relative Energies of [2′-Deoxythymidine phosphate]$^{2+\bullet}$ Isomers

	relative energy[a] (kJ mol^{-1})					
	gas phase			solvated		
ion[b]	B3LYP	M06-2X	ωB97X-D	B3LYP	M06-2X	ωB97X-D
21$^{+\bullet}$	0 (0)[c]	0 (0)[c]	0 (0)[c]	0 (0)[c]	0 (0)[c]	0 (0)[c]
22$^{+\bullet}$	16 (28)	3 (14)	8 (20)	3 (14)	−6 (5)	−2 (9)
23$^{+\bullet}$	7 (19)	−4 (8)	9 (21)	23 (33)	13 (22)	25 (35)
24$^{+\bullet}$	12 (22)	−8 (2)	7 (16)	27 (34)	−1 (6)	19 (26)
25$^{+\bullet}$	17 (25)	10 (18)	19 (27)	28 (29)	23 (31)	31 (39)

[a]Including B3LYP/6-31+G(d,p) zero-point energy corrections and referring to 0 K unless stated otherwise. [b]Lowest-energy conformers. [c]Relative free energies at 298 K.

DOI: 10.1021/acs.jpcb.7b09872
J. Phys. Chem. B 2018, 122, 86−97

existence of low-energy noncanonical nucleobase isomers of 2′-deoxythimidine phosphate cation radicals. It remains to be explored if such unusual species play a role in DNA ionization.

■ ASSOCIATED CONTENT

Supporting Information

The Supporting Information is available free of charge on the ACS Publications website at DOI: 10.1021/acs.jpcb.7b09872.

Complete ref 57, M06-2X/6-311+G(2d,p)-optimized geometries and total energies of thymine and thymidine cation radicals, UV−vis absorption spectra, CID mass spectra, D/H exchange kinetic plots, and RRKM rate constants (PDF)

■ AUTHOR INFORMATION

Corresponding Authors

*E-mail: ryzhov@niu.edu. Phone: 815-753-6955.
*E-mail: turecek@chem.washington.edu. Phone: 206-685-2041. Fax: 206-685-8665.

ORCID

František Tureček: 0000-0001-7321-7858

Notes

The authors declare no competing financial interest.

■ ACKNOWLEDGMENTS

Research at University of Washington was supported by the National Science Foundation Division of Chemistry (Grants CHE-1359810, CHE-1661815, and CHE-1624430) and the Klaus and Mary Ann Saegebarth Endowment. H.R. thanks the NSF-REU program (Grant CHE-1659548 to Northern Illinois University) for support.

■ REFERENCES

(1) Burrows, C. J.; Muller, J. G. Oxidative Nucleobase Modifications Leading to Strand Scission. *Chem. Rev.* **1998**, *98*, 1109−1151.
(2) Steenken, S. Purine Bases, Nucleosides, and Nucleotides: Aqueous Solution Redox Chemistry and Transformation Reactions of Their Radical Cations and e- and OH Adducts. *Chem. Rev.* **1989**, *89*, 503−520.
(3) Schuster, G. B. One-Electron Oxidation of DNA: Mechanism and Consequences. *Nucleic Acids Symp. Ser.* **2009**, *53*, 85−86.
(4) Kanvah, S.; Joseph, J.; Schuster, G. B.; Barnett, R. N.; Cleveland, C. L.; Landman, U. Oxidation of DNA: Damage to Nucleobases. *Acc. Chem. Res.* **2010**, *43*, 280−287.
(5) Murphy, C. J.; Arkin, M. R.; Jenkins, Y.; Ghatlia, N. D.; Bossmann, S. H.; Turro, N. J.; Barton, J. K. Long-Range Photoinduced Electron-Transfer through a DNA Helix. *Science* **1993**, *262*, 1025−1029.
(6) Giese, B. Hole Injection and Hole Transfer Through DNA: The Hopping Mechanism. *Top. Curr. Chem.* **2004**, *236*, 27−44.
(7) Saito, I.; Takayama, M.; Sugiyama, H.; Nakatani, K.; Tsuchida, A.; Yamamoto, M. Photoinduced DNA Cleavage Via Electron-transfer. Demonstration That Guanine Residues Located 5′ To Guanine Are the Most Electrondonating Sites. *J. Am. Chem. Soc.* **1995**, *117*, 6406−6407.
(8) Dougherty, D.; Wittel, K.; Meeks, J.; McGlynn, S. P. Photoelectron Spectroscopy of Carbonyls. Ureas, Uracils, and Thymine. *J. Am. Chem. Soc.* **1976**, *98*, 3815−3820.
(9) Fulfer, K. D.; Hardy, D.; Aguilar, A. A.; Poliakoff, E. D. High-Resolution Photoelectron Spectra of the Pyrimidine-Type Nucleobases. *J. Chem. Phys.* **2015**, *142*, 224310.
(10) Majdi, Y.; Hochlaf, M.; Pan, Y.; Lau, K.-C.; Poisson, L.; Garcia, G. A.; Nahon, L.; Al-Mogren, M. M.; Schwell, M. Theoretical and Experimental Photoelectron Spectroscopy Characterization of the Ground State of Thymine Cation. *J. Phys. Chem. A* **2015**, *119*, 5951−5958.
(11) Choi, K.-W.; Lee, J.-H.; Kim, S. K. Ionization Spectroscopy of a DNA Base: Vacuum-Ultraviolet Mass-Analyzed Threshold Ionization Spectroscopy of Jet-Cooled Thymine. *J. Am. Chem. Soc.* **2005**, *127*, 15674−15675.
(12) Ghosh, D.; Isayev, O.; Slipchenko, L. V.; Krylov, A. I. Effect of Solvation on the Vertical Ionization Energy of Thymine: From Microhydration to Bulk. *J. Phys. Chem. A* **2011**, *115*, 6028−6038.
(13) Improta, R.; Scalmani, G.; Barone, V. Radical Cations of DNA Bases: Some Insights on Structure and Fragmentation Patterns by Density Functional Methods. *Int. J. Mass Spectrom.* **2000**, *201*, 321−336.
(14) Close, D. M.; Crespo-Hernandez, C. E.; Gorb, L.; Leszczynski, J. Ionization Energy Thresholds (IETs) of Thymine, and Thymine Keto-Enol Tautomers. *J. Phys. Chem. A* **2006**, *110*, 7485−7490.
(15) Cauet, E.; Lievin, J. Radical Cations of the Nucleic Bases and Radiation Damage to DNA: Ab initio Study. *Adv. Quantum Chem.* **2007**, *52*, 121−147.
(16) Close, D. M.; Crespo-Hernandez, C. E.; Gorb, L.; Leszczynski, J. Theoretical Elucidation of Conflicting Experimental Data on Vertical Ionization Potentials of Microhydrated Thymine. *J. Phys. Chem. A* **2008**, *112*, 4405−4409.
(17) Seidel, C. A. M.; Schulz, A.; Sauer, M. H. M. Nucleobase-Specific Quenching of Fluorescent Dyes. 1. Nucleobase One-Electron Redox Potentials and Their Correlation with Static and Dynamic Quenching Efficiencies. *J. Phys. Chem.* **1996**, *100*, 5541−5553.
(18) Crespo-Hernandez, C. E.; Close, D. M.; Gorb, L.; Leszczynski, J. Determination of Redox Potentials for Watson-Crick Base Pairs, DNA Nucleosides, and Relevant Nucleoside Analogues. *J. Phys. Chem. B* **2007**, *111*, 5386−5395.
(19) Joy, A.; Ghosh, A. K.; Schuster, G. B. One-Electron Oxidation of DNA Oligomers That Lack Guanine: Reaction and Strand Cleavage at Remote Thymines by Long-Distance Radical Cation Hopping. *J. Am. Chem. Soc.* **2006**, *128*, 5346−5347.
(20) Ghosh, A.; Joy, A.; Schuster, G. B.; Douki, T.; Cadet, J. Selective One-Electron Oxidation of Duplex DNA Oligomers: Reaction at Thymines. *Org. Biomol. Chem.* **2008**, *6*, 916−928.
(21) Joseph, J.; Schuster, G. B. Oxidatively Damaged Nucleobases in Duplex DNA Oligomers: Reaction at Thymine-Thymine Mispairs. *J. Am. Chem. Soc.* **2009**, *131*, 13904−13905.
(22) Kanvah, S.; Schuster, G. B. One-Electron Oxidation of DNA: Thymine versus Guanine Reactivity. *Org. Biomol. Chem.* **2010**, *8*, 1340−1343.
(23) Kravec, S. M.; Kinz-Thompson, C. D.; Conwell, E. M. Localization of a Hole on an Adenine-Thymine Radical Cation in B-Form DNA in Water. *J. Phys. Chem. B* **2011**, *115*, 6166−6171.
(24) Barnett, R. N.; Joseph, J.; Landman, U.; Schuster, G. B. Oxidative Thymine Mutation in DNA: Water-Wire-Mediated Proton-Coupled Electron Transfer. *J. Am. Chem. Soc.* **2013**, *135*, 3904−3914.
(25) Wagner, J. R.; van Lier, J.-E.; Johnston, L. J. Quinone Sensitized Electron Transfer Photooxidation of Nucleic Acids: Chemistry of Thymine and Thymidine Radical Cations in Aqueous Solution. *Photochem. Photobiol.* **1990**, *52*, 333−343.
(26) Wagner, J. R.; van Lier, J. E.; Decarroz, C.; Berger, M.; Cadet, J. Photodynamic Methods for Oxyradical-Induced DNA Damage. *Methods Enzymol.* **1990**, *186*, 502−511.
(27) Douki, T.; Ravanat, J.-L.; Angelov, D.; Wagner, J. R.; Cadet, J. Effects of Duplex Stability on Charge-Transfer Efficiency within DNA. *Top. Curr. Chem.* **2004**, *236*, 1−25.
(28) Fujita, S.; Steenken, S. Pattern of OH Radical Addition to Uracil and Methyl- and Carboxyl-Substituted Uracils. Electron Transfer of OH Adducts with N,N,N′,N′-tetramethyl-p-phenylenediamine and Tetranitromethane. *J. Am. Chem. Soc.* **1981**, *103*, 2540−2545.
(29) Kim, N.-J. DFT Study of Water-Assisted Intramolecular Proton Transfer in the Tautomers of Thymine Radical Cation. *Bull. Korean Chem. Soc.* **2006**, *27*, 1009−1014.
(30) Kim, N. J.; Kim, H. M.; Kim, S. K. Ionization-Induced Proton Transfer in Thymine-Ammonia van der Waals Clusters. *Int. J. Mass Spectrom.* **2007**, *261*, 32−37.

DOI: 10.1021/acs.jpcb.7b09872
J. Phys. Chem. B 2018, 122, 86−97

(31) Heo, J.; Kim, N. J. DFT Study on the Nucleophilic Addition Reaction of Water and Ammonia to the Thymine Radical Cation. *J. Phys. Chem. A* **2007**, *111*, 8857−8863.
(32) Malone, M. E.; Symons, M. C. R.; Parker, A. W. An EPR Study of Photoionized Thymine and Its Derivatives at 77 K. *J. Chem. Soc., Perkin Trans. 2* **1993**, *2*, 2067−75.
(33) Yan, M.; Becker, D.; Summerfield, S.; Renke, P.; Sevilla, M. D. Relative Abundance and Reactivity of Primary Ion Radicals in γ-Irradiated DNA at Low Temperatures. 2. Single- vs Double-Stranded DNA. *J. Phys. Chem.* **1992**, *96*, 1983−1989.
(34) Sevilla, M. D. An Electron Spin Resonance Study of the Photoionization of Thymine. The Thymine Cation and Anion Radicals. *J. Phys. Chem.* **1971**, *75*, 626−631.
(35) Nishimoto, S.; Ide, H.; Wada, T.; Kagiya, T. Radiation-Induced Hydroxylation of Thymine Promoted by Electron-Affinic Compounds. *Int. J. Radiat. Biol. Relat. Stud. Phys., Chem. Med.* **1983**, *44*, 585−600.
(36) Sevilla, M. D. Electron Spin Resonance Study of N1-Substituted Thymine π-Cation Radicals. *J. Phys. Chem.* **1976**, *80*, 1898−1901.
(37) Rashid, R.; Mark, F.; Schuchmann, H. P.; Von Sonntag, C. Sulfate Anion Radical-Induced Oxidation of 1,3,6-Trimethyluracil and 1,3,5-Trimethyluracil (1,3-Dimethylthymine) by Potassium Peroxodisulfate in Aqueous Solution: An Interesting Contrast. *Int. J. Radiat. Biol.* **1991**, *59*, 1081−1100.
(38) Deeble, D. J.; Schuchmann, M. N.; Steenken, S.; Von Sonntag, C. Direct Evidence for the Formation of Thymine Radical Cations from the Reaction of Sulfate (SO4·-) with Thymine Derivatives: A Pulse Radiolysis Study with Optical and Conductance Detection. *J. Phys. Chem.* **1990**, *94*, 8186−8192.
(39) Itahara, T.; Fujii, Y.; Tada, M. Oxidation of Thymines by Peroxosulfate Ions in Water. *J. Org. Chem.* **1988**, *53*, 3421−3424.
(40) Adhikary, A.; Kumar, A.; Heizer, A. N.; Palmer, B. J.; Pottiboyina, V.; Liang, Y.; Wnuk, S. F.; Sevilla, M. D. Hydroxyl Ion Addition to One-Electron Oxidized Thymine: Unimolecular Interconversion of C5 to C6 OH-Adducts. *J. Am. Chem. Soc.* **2013**, *135*, 3121−3135.
(41) Tureček, F. Transient Intermediates of Chemical Reactions by Neutralization-Reionization Mass Spectrometry. *Top. Curr. Chem.* **2003**, *225*, 77−129.
(42) Yao, C.; Cuadrado-Peinado, M.; Polášek, M.; Tureček, F. Specific Generation of 1-Methylcytosine Radicals in the Gas-Phase. *Angew. Chem., Int. Ed.* **2005**, *44*, 6708−6711.
(43) Chen, X.; Syrstad, E. A.; Nguyen, M. T.; Gerbaux, P.; Turecek, F. Distonic Isomers and Tautomers of the Adenine Cation Radical in the Gas Phase and Aqueous Solution. *J. Phys. Chem. A* **2004**, *108*, 9283−9293.
(44) Wolken, J. K.; Syrstad, E. A.; Vivekananda, S.; Tureček, F. Uracil Radicals in the Gas Phase. Specific Generation and Energetics. *J. Am. Chem. Soc.* **2001**, *123*, 5804−5805.
(45) Tureček, F.; Julian, R. R. Peptide Radicals and Cation-Radicals in the Gas Phase. *Chem. Rev.* **2013**, *113*, 6691−6733.
(46) Korn, J. A.; Urban, J.; Dang, A.; Nguyen, H. T. H.; Turecek, F. UV-Vis Action Spectroscopy Reveals a Conformational Collapse in Hydrogen-Rich Dinucleotide Cation Radicals. *J. Phys. Chem. Lett.* **2017**, *8*, 4100−4107.
(47) Chu, I. K.; Rodriquez, C. F.; Lau, T.-C.; Hopkinson, A. C.; Siu, K. W. M. Molecular Radical Cations of Oligopeptides. *J. Phys. Chem. B* **2000**, *104*, 3393−3397.
(48) Wee, S.; O'Hair, R. A. J.; McFadyen, W. D. Can Radical Cations of the Constituents of Nucleic Acids Be Formed in the Gas Phase Using Ternary Transition Metal Complexes? *Rapid Commun. Mass Spectrom.* **2005**, *19*, 1797−1805.
(49) Feketeova, L.; Khairallah, G. N.; Chan, B.; Steinmetz, V.; Maitre, P.; Radom, L.; O'Hair, R. A. J. Gas-Phase Infrared Spectrum and Acidity of the Radical Cation of 9-Methylguanine. *Chem. Commun.* **2013**, *49*, 7343−7345.
(50) Lesslie, M.; Lawler, J. T.; Dang, A.; Korn, J. A.; Bím, D.; Steinmetz, V.; Maitre, P.; Tureček, F.; Ryzhov, V. Cytosine Radical Cation: A Gas-Phase Study Combining IRMPD Spectroscopy, UV-PD Spectroscopy, Ion−Molecule Reactions, and Theoretical Calculations. *ChemPhysChem* **2017**, *18*, 1293−1301.
(51) Feketeova, L.; Chan, B.; Khairallah, G. N.; Steinmetz, V.; Maitre, P.; Radom, L.; O'Hair, R. A. J. Gas-Phase Structure and Reactivity of the Keto Tautomer of the Deoxyguanosine Radical Cation. *Phys. Chem. Chem. Phys.* **2015**, *17*, 25837−25844.
(52) Feketeova, L.; Chan, B.; Khairallah, G. N.; Steinmetz, V.; Maitre, P.; Radom, L.; O'Hair, R. A. J. Watson-Crick Base Pair Radical Cation as a Model for Oxidative Damage in DNA. *J. Phys. Chem. Lett.* **2017**, *8*, 3159−3165.
(53) Antoine, R.; Dugourd, P. UV-Visible Activation of Biomolecular Ions. (Laser Photodissociation and Spectroscopy of Mass-Separated Biomolecular Ions). *Lect. Notes Chem.* **2013**, *83*, 93−116.
(54) Lam, A. K.; Abrahams, B. F.; Grannas, M. J.; McFadyen, W. D.; O'Hair, R. A. J. Tuning the Gas Phase Redox Properties of Copper(II) Ternary Complexes of Terpyridines to Control the Formation of Nucleobase Radical Cations. *Dalton Trans.* **2006**, 5051−5061.
(55) Shaffer, C. J.; Pepin, R.; Tureček, F. Combining UV Photodissociation Action Spectroscopy with Electron Transfer Dissociation for Structure Analysis of Gas-Phase Peptide Cation-Radicals. *J. Mass Spectrom.* **2015**, *50*, 1438−1442.
(56) Pyatkivskyy, Y.; Ryzhov, V. Coupling of Ion−Molecule Reactions with Liquid Chromatography on a Quadrupole Ion Trap Mass Spectrometer. *Rapid Commun. Mass Spectrom.* **2008**, *22*, 1288−1294.
(57) Frisch, M. J.; Trucks, G. W.; Schlegel, H. B.; Scuseria, G. E.; Robb, M. A.; Cheeseman, J. R.; Scalmani, G.; Barone, V.; Mennucci, B.; Petersson, G. A.; Nakatsuji, H.; Caricato, M.; Li, X.; Hratchian, H. P.; Izmaylov, A. F.; Bloino, J.; Zheng, G.; Sonnenberg, J. L.; Hada, M.; Ehara, M.; Toyota, K.; Fukuda, R.; Hasegawa, J.; Ishida, M.; Nakajima, T.; Honda, Y.; Kitao, O.; Nakai, H.; Vreven, T.; Montgomery, J. A., Jr.; Peralta, J. E.; Ogliaro, F.; Bearpark, M.; Heyd, J. J.; Brothers, E.; Kudin, K. N.; Staroverov, V. N.; Keith, T.; Kobayashi, R.; Normand, J.; Raghavachari, K.; Rendell, A.; Burant, J. C.; Iyengar, S. S.; Tomasi, J.; Cossi, M.; Rega, N.; Millam, J. M.; Klene, M.; Knox, J. E.; Cross, J. B.; Bakken, V.; Adamo, C.; Jaramillo, J.; Gomperts, R.; Stratmann, R. E.; Yazyev, O.; Austin, A. J.; Cammi, R.; Pomelli, C.; Ochterski, J. W.; Martin, R. L.; Morokuma, K.; Zakrzewski, V. G.; Voth, G. A.; Salvador, P.; Dannenberg, J. J.; Dapprich, S.; Daniels, A. D.; Farkas, Ö.; Foresman, J. B.; Ortiz, J. V.; Cioslowski, J.; Fox, D. J. *Gaussian 09*, revision A.02; Gaussian Inc.: Wallingford, CT, 2009.
(58) Becke, A. D. New Mixing of Hartree-Fock and Local Density-Functional Theories. *J. Chem. Phys.* **1993**, *98*, 1372−1377.
(59) Zhao, Y.; Truhlar, D. G. The M06 Suite of Density Functionals for Main Group Thermochemistry, Thermochemical Kinetics, Noncovalent Interactions, Excited States, and Transition Elements: Two New Functionals and Systematic Testing of Four M06-Class Functionals and 12 Other Functionals. *Theor. Chem. Acc.* **2008**, *120*, 215−241.
(60) Chai, J. D.; Head-Gordon, M. Long-Range Corrected Hybrid Density Functionals with Damped Atom-Atom Dispersion Corrections. *Phys. Chem. Chem. Phys.* **2008**, *10*, 6615−6620.
(61) Tomasi, J.; Mennucci, B.; Cammi, R. Quantum Mechanical Continuum Solvation Models. *Chem. Rev.* **2005**, *105*, 2999−3093.
(62) Møller, C.; Plesset, M. S. A Note on an Approximation Treatment for Many Electron Systems. *Phys. Rev.* **1934**, *46*, 618−622.
(63) Dunning, T. H., Jr Gaussian Basis Sets for Use in Correlated Molecular Calculations. I. The Atoms Boron Through Neon and Hydrogen. *J. Chem. Phys.* **1989**, *90*, 1007−1023.
(64) Schlegel, H. B. Potential Energy Curves Using Unrestricted M? ller-Plesset Perturbation Theory with Spin Annihilation. *J. Chem. Phys.* **1986**, *84*, 4530.
(65) Mayer, I. Spin-Projected UHF Method. IV. Comparison of Potential Curves Given by Different One-Electron Methods. *Adv. Quantum Chem.* **1980**, *12*, 189−262.
(66) Chan, B.; Radom, L. Assessment of Theoretical Procedures for Hydrogen Atom Abstraction by Chlorine, and Related Reactions. *Theor. Chem. Acc.* **2011**, *130*, 251−260.
(67) Cížek, J. On the Use of the Cluster Expansion and the Technique of Diagrams in Calculations of Correlation Effects in Atoms and Molecules. *Adv. Chem. Phys.* **1969**, *14*, 35−89.

DOI: 10.1021/acs.jpcb.7b09872
J. Phys. Chem. B 2018, 122, 86−97

(68) Purvis, G. D., III; Bartlett, R. J. A. Full Coupled-Cluster Singles and Doubles Model — the Inclusion of Disconnected Triples. *J. Chem. Phys.* **1982**, *76*, 1910—1918.
(69) Sekino, H.; Bartlett, R. J. A Linear Response, Coupled-Cluster Theory for Excitation Energy. *Int. J. Quantum Chem.* **1984**, *26*, 255—265.
(70) Comeau, D. C.; Bartlett, R. J. The Equation-of-Motion Coupled-Cluster Method. Applications to Open- and Closed-Shell Reference States. *Chem. Phys. Lett.* **1993**, *207*, 414—423.
(71) Furche, F.; Ahlrichs, A. Adiabatic Time-Dependent Density Functional Methods for Excited State Properties. *J. Chem. Phys.* **2002**, *117*, 7433—7447.
(72) Turecek, F. Benchmarking Electronic Excitation Energies and Transitions in Peptide Radicals. *J. Phys. Chem. A* **2015**, *119*, 10101—10111.
(73) Nguyen, H. T. H.; Andrikopoulos, P. C.; Bím, D.; Rulíšek, L.; Dang, A.; Tureček, F. Radical Reactions Affecting Polar Groups in Threonine Peptide Ions. *J. Phys. Chem. B* **2017**, *121*, 6557—6569.
(74) Barbatti, M.; Ruckenbauer, M.; Plasser, F.; Pittner, J.; Granucci, G.; Persico, M.; Lischka, H. Newton-X: A Surface-Hopping Program for Nonadiabatic Molecular Dynamics. Wiley Interdisciplinary Reviews: *Comput. Mol. Sci.* **2014**, *4*, 26—33.
(75) Gilbert, R. G.; Smith, S. C. *Theory of Unimolecular and Recombination Reactions*; Blackwell Scientific Publications: Oxford, U.K., 1990; pp 52—132.
(76) Zhu, L.; Hase, W. L. *Program No. QCPE 644*; Quantum Chemistry Program Exchange, Indiana University: Bloomington, IN, 1994.
(77) Frank, A. J.; Sadílek, M.; Ferrier, J. G.; Tureček, F. Sulfur Oxoacids and Radicals in the Gas Phase. A Variable-Time Neutralization-Photoexcitation-Reionization Mass Spectrometric and Ab Initio/RRKM Study. *J. Am. Chem. Soc.* **1997**, *119*, 12343—12353.
(78) Ulrich, J.; Teoule, R.; Massot, R.; Cornu, A. Mass-Spectrometric Study of the Fragmentation of Uracil and Thymine Derivatives. *Org. Mass Spectrom.* **1969**, *2*, 1183—99.
(79) Imhoff, M.; Deng, Z.; Huels, M. A. Identification of Ion Fragments Produced from Thymine and Deuterated Thymine by Low Energy Ion Impact in Films and Electron Impact in the Gas Phase. *Int. J. Mass Spectrom.* **2005**, *245*, 68—77.
(80) Almeida, D.; Antunes, R.; Martins, G.; Eden, S.; Ferreira da Silva, F.; Nunes, Y.; Garcia, G.; Limao-Vieira, P. Electron Transfer-Induced Fragmentation of Thymine and Uracil in Atom-Molecule Collisions. *Phys. Chem. Chem. Phys.* **2011**, *13*, 15657—15665.
(81) Thymine Mass Spectrum. In *NIST Chemistry WebBook*; NIST Standard Reference Database 69; National Institute of Standards and Technology (NIST): Gaithersburg, MD, 2005; available at http://webbook.nist.gov/chemistry (accessed October 20, 2017).
(82) Meotner, M. Charge Transfer Equilibria and Complexes. In *The Encyclopedia of Mass Spectrometry*; Gross, M. L., Caprioli, R., Eds; Elsevier: Amsterdam, 2003; Vol. *1*, Theory and Ion Chemistry, pp 345—350.
(83) Barbatti, M.; Aquino, A. J. A.; Lischka, H. The UV Absorption of Nucleobases: Semi-Classical Ab Initio Spectra Simulations. *Phys. Chem. Chem. Phys.* **2010**, *12*, 4959—4967.
(84) Rejnek, J.; Hanus, M.; Kabelac, M.; Ryjacek, F.; Hobza, P. Correlated Ab Initio Study of Nucleic Acid Bases and Their Tautomers in the Gas Phase, in a Microhydrated Environment and in Aqueous Colution. Part 4. Uracil and Thymine. *Phys. Chem. Chem. Phys.* **2005**, *7*, 2006—2017.
(85) Jiao, D.; Wang, H.; Zhang, Y.; Tang, Y. A DFT Study of Thymine and Its Tautomers. *Can. J. Chem.* **2009**, *87*, 406—415.

DOI: 10.1021/acs.jpcb.7b09872
J. Phys. Chem. B 2018, 122, 86—97